

An Abrupt Transition in the Mechanical Response of the Upper Crust to Transpression along the Queen Charlotte Fault

by Anne M. Tréhu, Maren Scheidhauer,* Kristin M. M. Rohr, Basil Tikoff, Maureen A. L. Walton, Sean P. S. Gulick, and Emily C. Roland

Abstract The Queen Charlotte Fault (QCF) is a major strike-slip fault that forms the boundary between the Pacific and North American plates from 51° to 58° N. Near 53.2° N, the angle of oblique convergence predicted by the Mid-Ocean Ridge VElocity (MORVEL) interplate pole of rotation decreases from > 15° in the south to < 15° in the north. South of 53.2° N, the convergent component of plate motion results in the formation of a 40 km wide terrace on the Pacific plate west of QCF and earthquakes with thrust mechanisms (including the 2012 Haida Gwaii earthquake sequence) are observed. North of 53.2° N, in the primary rupture zone of the M 8.1 strike-slip earthquake of 1949, the linear terrace disappears, and topography of the continental slope west of the QCF is characterized by a complex pattern of ridges and basins that trend obliquely to the primary trace of the QCF. Deformation within the Pacific plate appears to occur primarily through strike-slip faulting with a minor thrust component on secondary synthetic faults. The orientations of these secondary faults, as determined from seismic reflection and bathymetric data, are consistent with the reactivation of faults originally formed as ridge-parallel normal faults and as thrust faults formed parallel to the QCF south of the bend at 53.2° N and subsequently translated to the north. We suggest that an oblique convergence angle of 15° represents a critical threshold separating distinct crustal responses to transpression. This result is consistent with theoretical and analog strain models of transpressive plate boundaries. The sharpness of this transition along the QCF, in contrast to purely continental transform boundaries, may be facilitated by the relatively simple structure of oceanic crust and the presence of pre-existing, optimally oriented faults in the young Pacific plate.

Introduction

Transpression is characteristic of dominantly transform plate boundaries that have a component of convergence (e.g., Sanderson and Marchini, 1984; McCaffrey, 1992; Fossen *et al.*, 1994; Braun and Beaumont, 1995; Walcott, 1997; Fossen and Tikoff, 1998; Chéry *et al.*, 2001). Analytical, numerical, and experimental studies indicate the angle of convergence should have a critical influence on the resulting transpressional deformation. Fossen and Tikoff (1993, 1998) argue on the basis of analytical models for finite and infinitesimal strain that a transition in behavior should occur at an angle of oblique convergence of 20° (Fig. 1). For lower angles of oblique collision (< 20°), deformation should be characterized as simple shear-dominated transpression, and the inferred minimum compressive stress should lie in the horizontal plane. In contrast, pure shear-dominated deformation should occur at oblique conver-

gence angles > 20°, characterized by a vertical minimum compressive stress resulting in thrust faults that are parallel to the main strike-slip fault. The numerical models of Braun and Beaumont (1995) also indicate a change in behavior for angles of oblique convergence of 15°–20°.

Analog models in which the deformation of brittle (dry sand) and/or ductile (silicone putty) layers is documented in response to forcing by motion of a rigid base (Burbridge and Braun, 1998; Casas *et al.*, 2001) show behavior that is generally consistent with these theoretical results. In the Burbridge and Braun (1998) model, a Mylar sheet forming the base of one plate was pulled at a series of oblique angles through a slit in the middle of the base of the model box. In contrast, in the Casas *et al.* (2001) model, a thin plastic plate that extended halfway across the model box was pushed from the side. For both models, the properties and thickness of the sand and the relative velocity of the basal layer were scaled to represent upper crustal deformation in response to oblique relative motion of underlying tectonic plates. The full range

*Now at Risk Management Solutions Limited, Zweigniederlassung Zürich, Stampfenbachstrasse 85, CH-8006, Zürich, Switzerland.

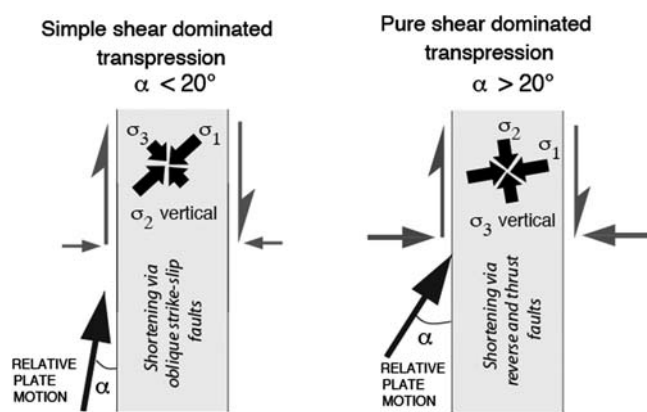


Figure 1. Schematic illustration of the stress field when the angle of convergence is $< 20^\circ$ and when it is $> 20^\circ$ as predicted by the theory of Fossen and Tikoff (1993, 1998). Gray vectors shown the shear and normal components of the relative plate motion vector.

of transpression was explored, from pure convergent to pure transcurrent relative motion. Although the geometry of the discontinuity in particle velocity at depth was different for the two experiments, a change in behavior was observed in both at an angle of oblique convergence of 15° – 25° . As the angle of oblique convergence decreased through this threshold, the structure of a mature plate boundary changed from discrete thrust and strike-slip faults with similar strikes to dominantly strike-slip deformation along a through-going fault accompanied by oblique strike-slip faults.

In nature, additional variables can affect how transpression is accommodated. These include heterogeneities in the rheology along and across the plate boundary, the presence and orientation of pre-existing faults, and the possibility of postfaulting rotations that obscure the original structural relationship between faults. As a major transpressive plate boundary, the Queen Charlotte Fault (QCF) system is similar to the San Andreas fault system of California (e.g., Wallace, 1990) and the Alpine fault in New Zealand (e.g., Walcott, 1997). However, the QCF is different from these well-studied fault systems in that it juxtaposes young oceanic lithosphere with thin, mafic, and recently extended continental lithosphere and therefore minimizes the impact of these additional variables (Lewis *et al.*, 1991; Rohr *et al.*, 2000; Smith *et al.*, 2003).

Tectonic Setting and Morphology of the QCF System

Plate Motions: Past and Present

The QCF system offshore western Canada and southeast Alaska is a major transform plate boundary that separates the Pacific and North American plates (Fig. 2a). It extends over 800 miles from near the southern tip of Haida Gwaii (formerly Queen Charlotte Islands) to the Yakutat block offshore of southeast Alaska. The continental slope west of the QCF is known as the Queen Charlotte Terrace (QCT; Fig. 2b). From 52° to 54° N, the terrace is flanked to the southwest by a

topographic depression in the deep ocean floor known as the Queen Charlotte Trough. This article focuses on the terrace, and a companion paper (Walton *et al.*, 2015) focuses on the trough. Rohr *et al.* (2000) discussed the broader regional context of the seismic reflection data presented here.

Smith *et al.* (2003) reviewed several different reconstructions of the plate tectonic history of the QCF. Prior to 40 Ma, the plate boundary was a subduction zone, with either the Pacific or the Kula plate being subducted (Hyndman and Hamilton, 1993). Since 40 Ma, the plate boundary has been primarily transcurrent, with likely, but poorly constrained, episodes of both transpression and transtension (Rohr and Currie, 1997; Smith *et al.*, 2003). Timing of the initiation of the current episode of contraction has long been debated. Most estimates have been between 8 and 3.4 Ma (Cox and Engebretson, 1985; Stock and Molnar, 1988; Atwater and Stock, 1998). The most recent estimates range between 5 and 6 Ma (Wilson, 2002; Smith *et al.*, 2003; Doubrovine and Tarduno, 2008).

The plate motion vectors predicted by the Mid-Ocean Ridge VELOCITY (MORVEL) global plate motion model (DeMets *et al.*, 2010), which represents current motions averaged over ~ 1 Ma, are shown in Figure 2 with the length scaled to show the predicted amount of relative motion accumulated over 6 Ma. The position of the QCF in Figure 2 was picked from digital images of the GLORIA sidescan data with 50 megapixel resolution (Bruns *et al.*, 1992), where it appears as a narrow lineation that runs along the continental slope and shelf. The fault has discrete changes in orientation near 53.2° and 54.3° N (see fig. 2 in Rohr *et al.*, 2000). Given uncertainties in how much Pacific/North America plate motion is taken up by deformation within western North America and whether the MORVEL rate has been constant for the past 5–6 Ma, this is only an approximate estimate of the area of potential overlap that must be accommodated either through underthrusting of the Pacific plate (Hyndman and Hamilton, 1993; Smith *et al.*, 2003; Bustin *et al.*, 2007), thickening of the plates adjacent to the QCF (Mackie *et al.*, 1989; Rohr *et al.*, 2000), or some combination thereof. Because the Pacific/North America late motion vectors along the QCF predicted by MORVEL are approximately the same length but rotated $\sim 5^\circ$ counterclockwise compared with the vectors predicted by NUVEL-1A (DeMets *et al.*, 1994), the amount of contraction that must be accommodated over the past 5–6 Ma is 50%–80% less than that assumed in previous studies.

The direction and rate of plate motion between the Pacific and North American plates along the QCF from 52° to 58° N are shown in Figure 3a. The pole of rotation is sufficiently far away that the rate and direction do not change significantly over this 660 km length of plate boundary. The component of compression across the plate boundary and the angle between the predicted relative motion vector and the local orientation of the QCF are shown in Figure 3b. The changing strike of the QCF results in a decreasing amount of shortening to the north with discrete changes at bends in the fault. North of 54.3° N, the angle of oblique convergence is approximately constant at 5° .

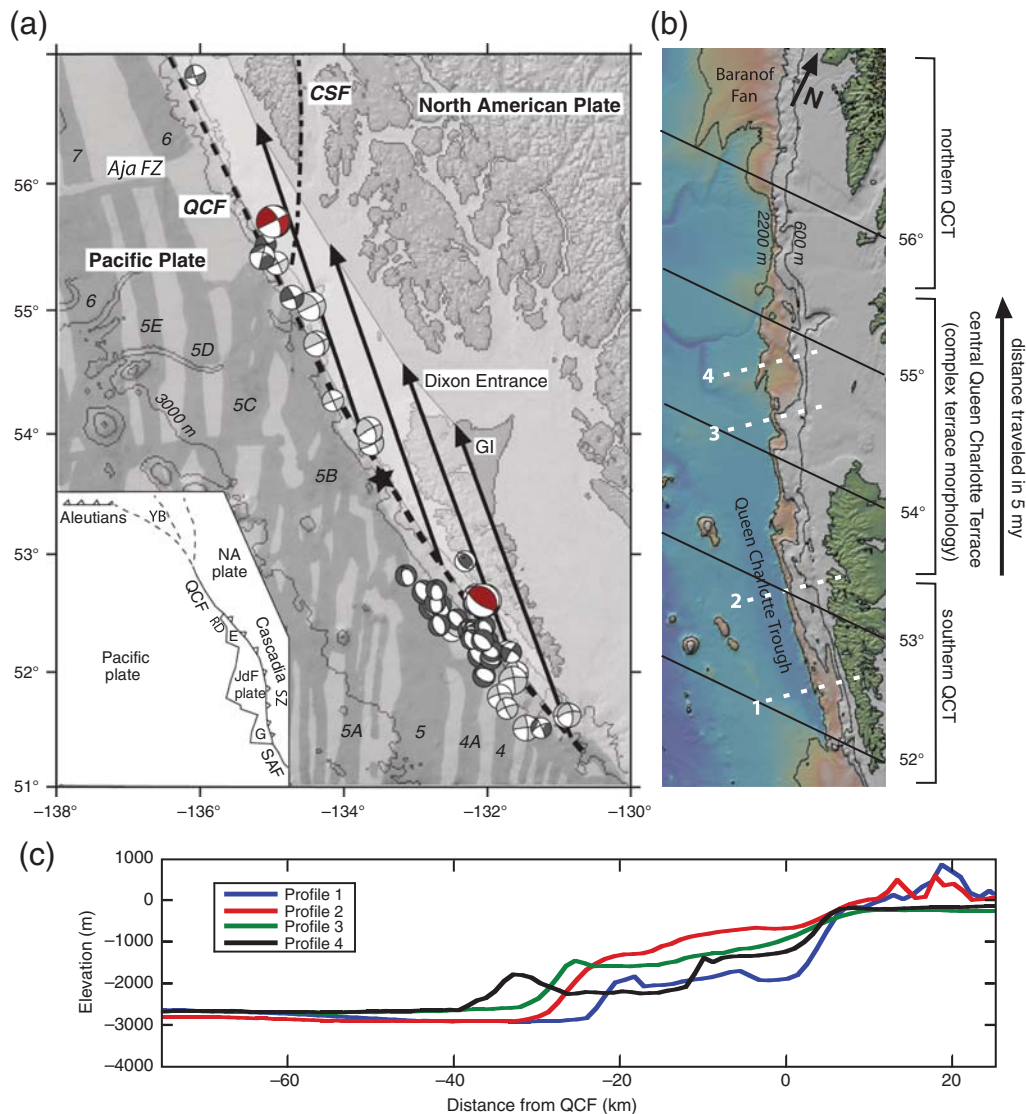


Figure 2. (a) Regional map showing the location of the Queen Charlotte fault (QCF) and Chatham straight fault (CSF). Offshore magnetic anomalies are shaded and labeled 4–7 (from [Atwater, 1989](#)). Bathymetric contours are shown at 1000 m intervals. Bathymetry for (a), (b), and (c) is from the global multiresolution topography (GMRT) database (see [Data and Resources](#)). Earthquake mechanisms are from the Global Centroid Moment Tensor (CMT) catalog for 1976–2013 ([Ekström et al., 2012](#)). The 28 October 2012 Haida Gwaii and 5 January 2013 Craig earthquakes are shown with compressional quadrants in red; events postdating these are shown in dark gray; mechanisms of previous events are shown in light gray. The star shows the epicenter of the 1949 M 8.1 event ([Bostwick, 1984](#)). The location of the QCF was digitized from GLORIA sidescan data ([Bruns et al., 1992](#)). Relative Pacific/North America plate motion vectors, scaled to show the predicted amount of plate overlap accumulated in 6 million years assuming the Mid-Ocean Ridge VELOCITY (MORVEL) model of [DeMets et al. \(2010\)](#), are also shown with the area of potential overlap highlighted. The inset shows the regional plate tectonic setting (adapted from [Riddihough and Hyndman, 1991](#)). E, Explorer plate; JdF, Juan de Fuca; RD, Revere-Delwood fault; G, Gorda plate; SAF, San Andreas fault; QCF, Queen Charlotte fault; Aja FZ, Aja fracture zone; YB, Yakutat block; GI, Graham Island. Graham Island is the northernmost, and largest, of a group of islands between 52° and 54° N that are collectively referred to as Haida Gwaii. (b) Morphology of the Queen Charlotte terrace (QCT) as defined by the 600, 1400, and 2200 m isobaths overlain on color-shaded bathymetry. Zones characterized by different deformation styles are also indicated. White dashed lines are the location of representative topographic profiles across the QCT shown in (c).

The age of the Pacific plate adjacent to the QCF is shown in Figure 3c and increases to the north from ~6.5 to 22 Ma, with the strongest gradient in plate age between 52 and 54° N. This age difference corresponds to an expected change in the thickness of the thermally defined plate from 27 to 39 km and an expected increase in water depth of 400 m in this segment

([Turcotte and Schubert, 1982](#)). This expected increase in water depth, however, is not observed because of thickening sediment to the north due to the presence of the Baranof Fan ([Walton et al., 2014](#)). The corresponding change in elastic plate thickness, considering the base of the elastic plate to be at 600°C, as is appropriate for an oceanic mantle composition, is 13–18 km.

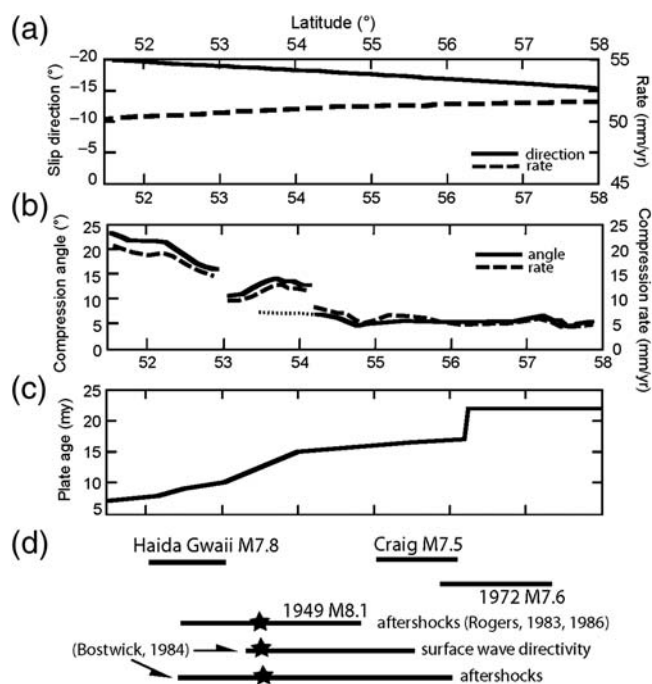


Figure 3. (a) Direction and rate of Pacific plate motion relative to North America for the MORVEL model (DeMets *et al.*, 2010). (b) The angle of compression between the predicted Pacific/North American plate motion vector of (a) and the local orientation of the QCF. The local orientation of the QCF was digitized from GLORIA sidescan data and smoothed with a running average of three points. The dotted line from 53.4° to 54° corresponds to the possible former trace of the QCF shown in Figure 5. (c) The age of the Pacific plate adjacent to the QCF from the magnetic anomaly picks of Atwater (1989) shown in Figure 1. (d) The rupture extent of historic large earthquakes along the QCF determined from the aftershock distribution. For the 1949 earthquake, the extent determined from surface-wave directivity analysis is shown as well as two different models based on aftershocks (Rogers, 1983, 1986; Bostwick, 1984). The extent of rupture determined from directivity is significantly smaller than that suggested by the aftershock distribution. Data to constrain fault termination points for the 1949 earthquake are quite limited, and all estimates are within the uncertainty for moment/length scaling relationships for strike-slip earthquakes (Leonard, 2010).

Historic and Recent Earthquake Activity

Over the past 70 years, most of the QCF has ruptured during large $M > 7$ earthquakes (Ristau *et al.*, 2007). Our study area covers a segment of the fault that ruptured in 1949 in an M 8.1 earthquake that was the largest earthquake in the recorded history to occur in Canada. The recent Haida Gwaii and Craig earthquakes occurred near the southern and northern ends, respectively, of the 1949 rupture. To first order, the northern extent of rupture during the Haida Gwaii earthquake and the southern extent of rupture during the Craig earthquake correspond to structural transitions discussed in this article.

The epicenter of the 1949 event is shown as a star in Figures 2–4. The limited data available at the time of the earthquake indicated a strike-slip mechanism with a strike of 325° on a nearly vertical fault (Rogers, 1983; Bostwick,

1984). This orientation is consistent with the local strike of the QCF apparent in GLORIA backscatter images (Bruns *et al.*, 1992; Rohr *et al.*, 2000). Aftershocks suggest a bilateral rupture pattern, although the northern extent of rupture is debated; Rogers (1983, 1986) suggested that aftershocks extended from 52.2° to 54.8° N based primarily on data recorded at seismic station VIC (Victoria, British Columbia), whereas Bostwick (1984) concluded that aftershocks extended north to ~56° N based on S – P times from seismic station SIT (Sitka, Alaska). In contrast to the rupture length suggested by the aftershock distribution, analysis of surface-wave directivity suggests a unilateral rupture that extended northward ~265 km to 55.5° N (Bostwick, 1984), an interpretation supported by a reanalysis of old seismograms by Lay *et al.* (2013). These various estimates for the extent of rupture in 1949 are shown schematically in Figure 3d. Bostwick (1984) interpreted the mismatch in fault length determined through the two independent techniques to indicate that the amount of slip was small at the southern and northern ends of the rupture zone defined by aftershocks.

Other major historic earthquakes along the margin include an M 7.9 event in 1958 along the northern extent of the fault (north of ~57.5° N, where the QCF name changes to the Fairweather fault) (Doser and Rodriguez, 2011) and an M 7.6 event with a strike of 340° that ruptured from 56° to 57.5° N (Schell and Ruff, 1989). These events also appear to have slipped on near-vertical, right-lateral strike-slip faults.

Recently, the M 7.8 Haida Gwaii earthquake in October 2012 and the M 7.5 Craig, Alaska, earthquake in January 2013 occurred on the QCF at opposite ends of the segment that ruptured in 1949 as defined by the surface-wave directivity analysis (Bostwick, 1984). In addition to providing a new suite of modern seismic observations to constrain earthquake source properties, these events highlight the variability in fault geometry and stress orientation along strike. During the 2012 Haida Gwaii earthquake, which occurred south of 53° N, slip occurred on a low-angle (~18°–25°) thrust fault dipping to the east that appears to strike parallel to the primary strike-slip fault trace based on the centroid moment tensor (CMT) solution (Lay *et al.*, 2013). Although the presence of earthquakes with thrust mechanisms west of the main strand of the QCF in this region had been documented prior to the earthquake (e.g., Ristau *et al.*, 2007), the Haida Gwaii thrust event was surprising because of its large magnitude. Strike-slip movement on the main strand of the QCF was notably absent during the Haida Gwaii earthquake sequence. As discussed above, it is likely that aftershocks of the 1949 earthquake extended into this region, but it is uncertain how much slip occurred on the QCF during the mainshock and whether the expected strike-slip component of plate motion is accommodated aseismically or in rare, large events (Lay *et al.*, 2013).

Another surprising feature of the Haida Gwaii sequence was the large number of normal-faulting aftershocks that occurred in the Pacific plate west of the QCF after the mainshock (Figs. 4 and 5). Such aftershocks are common for

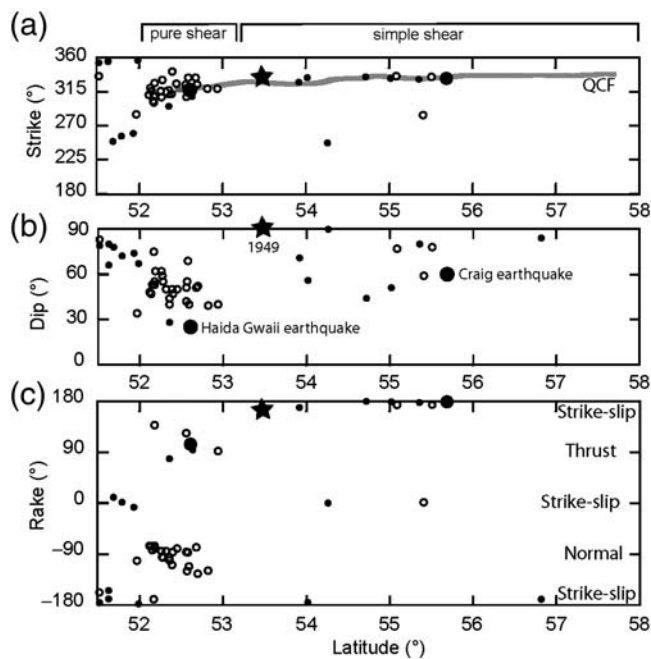


Figure 4. (a) Strike, (b) dip, and (c) rake for earthquakes shown in Figure 2a from the CMT catalog (see [Data and Resources](#)). Large black circles indicate the Haida Gwaii and Craig earthquakes; star is the 1949 earthquake; small black circles are events prior to October 2012; and open circles postdate the Haida Gwaii event. The gray line shows the local strike of the QCF. In spite of a large range of fault dips and mechanisms that include strike-slip, reverse, and normal faulting, strikes for most events north of 52° N are very close to the local strike of the QCF. South of 52°, the orientation of earthquake fault planes appears to be controlled by other structural features (see [Rohr, 2015](#)). (All CMT solutions include two orthogonal nodal planes. The plane with the orientation closest to the strike of the QCF was chosen to represent the fault plane. If strikes were randomly oriented, deviations up to 90° from the local strike of the QCF would be observed.)

large subduction zone thrust earthquakes that result from bending of the subducted plate (e.g., [Christensen and Ruff, 1988](#); [Lay et al., 2011](#)). The region of normal faulting is at the southern end of a broad depression in seafloor topography known as the Queen Charlotte Trough (Fig. 2b). [Walton et al. \(2015\)](#) describe buried, presently inactive, normal faults as far north as 54° N, suggesting that normal faulting that occurs southwest of Haida Gwaii is translated north with the Pacific plate.

The 2013 Craig earthquake was a steeply dipping strike-slip event near the northern termination of the 1949 rupture. This earthquake was surprising in that the rupture velocity during the main event may have exceeded the shear-wave velocity ([Yue et al., 2013](#)), possibly resulting from a strong contrast in material properties across the ocean-continent fault. Aftershocks of this event indicate that slip occurred along a steeply dipping fault plane at depths consistent with the elastic thickness predicted for ~16 my old oceanic lithosphere, although a handful of aftershocks (including the largest aftershock, an M 5.9 event that occurred 25 days after

the mainshock) may have occurred off the primary fault trace with focal mechanisms that indicate some variability in source properties ([Ruppert et al., 2014](#)). The southern end of the Craig rupture, near 55° N, is located where the amount of convergence across the QCF changes (Fig. 3) and is coincident with the northern extent of the region of secondary wrench faulting in the Pacific plate that we document in this study. The northern extent of the Craig rupture, near 56° N, appears to coincide with the southern end of rupture in the 1972 Sitka earthquake ([Schell and Ruff, 1989](#)) and with the Aja fracture zone in the Pacific plate, indicated in Figure 2 by an offset in the magnetic anomalies.

Fault mechanisms from CMT solutions ([Ekström et al., 2012](#)) for all events with $M > 5$ since 1976 are shown in Figure 2. The uncertainty in these hypocentral parameters is discussed in other articles of this volume and does not affect our conclusions. Figure 4 shows the strike, dip, and rake of these CMT solutions compared with the strike of the QCF. Additional regional moment tensor solutions show a similar pattern ([Ristau et al., 2007](#)). It is clear that the highest level of seismic activity and greatest diversity of mechanisms for these historical events occur between 52° and 53° N. Both thrust and strike-slip mechanisms along this segment of the QCF have strikes similar to the local strike of the QCF ([Berube et al., 1989](#); [Rohr and Furlong, 1995](#); [Braunmiller and Nabelek, 2002](#); [Ristau et al., 2007](#); [Rohr and Tryon, 2010](#)), consistent with pure shear-dominated transpression (Fig. 1).

Morphology of the Queen Charlotte Terrace

The QCT, approximated in Figure 2b as the region between the 600 and 2200 m bathymetric contours, is the dominant morphological feature of the continental margin in this region. The central section is shown in more detail in Figure 5. The morphology of the terrace varies considerably along strike. Where the oblique component of plate motion is greatest, from 52° to 53.2° N (which we refer to as the southern QCT), the continental margin is characterized by a 30 km wide terrace bounded by nearly parallel scarps ([Chase and Tiffin, 1972](#); [Hyndman and Ellis, 1981](#)). South of 52° N, the margin morphology is affected by northward propagation of the Revere-Dellwood fault (Fig. 2a, inset; [Rohr, 2015](#)). Seismicity ([Hyndman and Ellis, 1981](#)) and GLORIA sidescan data ([Bruns et al., 1992](#)) indicate that the scarp on the northeast side of the QCT corresponds to the primary trace of the QCF. Although recent larger earthquakes, including the 2012 Haida Gwaii event, exhibit thrust-fault focal mechanisms, in general, earthquakes along this portion of the QCF show both strike-slip and thrust-fault focal mechanisms with nodal planes that strike approximately parallel to the QCF (Fig. 4). Ridges on the seafloor within the terrace are also consistent with shortening perpendicular to the QCF. These observations suggest that strain is partitioned between strike-slip motion on a nearly vertical strike-slip fault (the QCF) and reverse motion on sub-parallel thrust and reverse faults within the Pacific plate, as

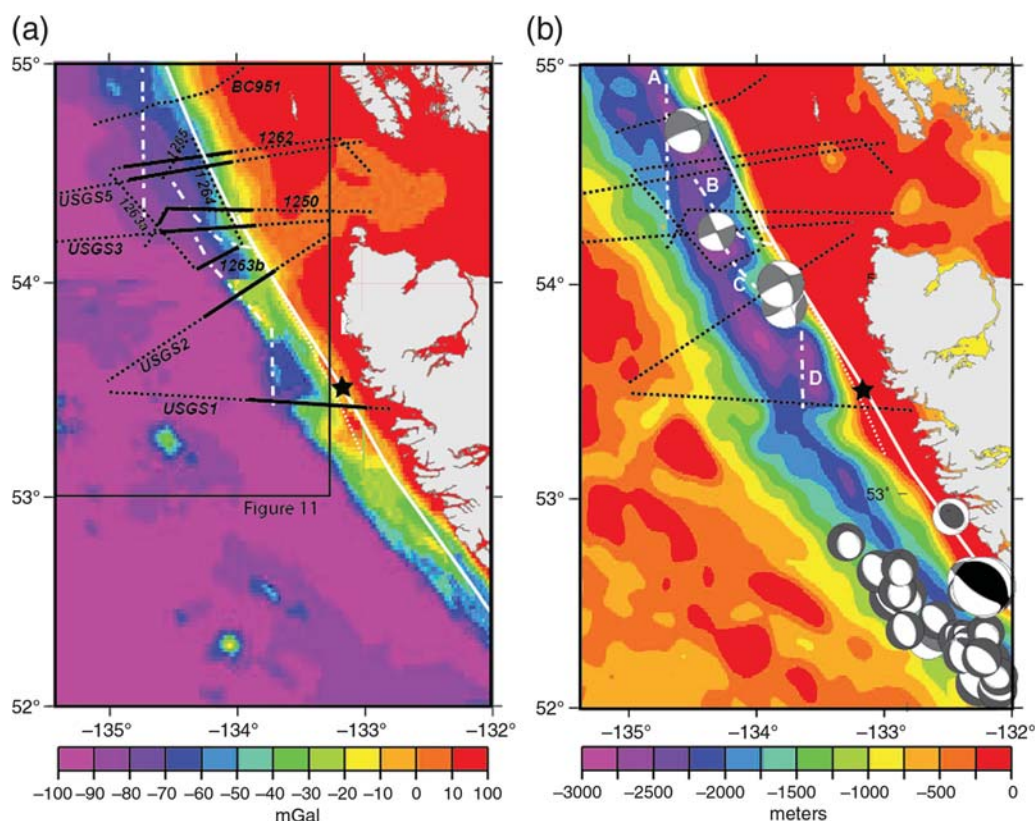


Figure 5. (a) Free-air gravity from GEOSAT and (b) regional bathymetry with CMT mechanisms overlain. Locations of multichannel seismic reflection profiles acquired by the U.S. Geological Survey (USGS) or the ACCRETE project are shown as dashed black lines on both maps and are labeled in (a); portions of profiles shown in Figure 6 are highlighted by a solid black line. The main strand of the QCF is shown as a solid white line on both maps. Fault zones A–D are shown as dashed white lines and labeled in (b). A possible inactive strand of the QCF is shown as a dotted white line south of 54° N. (Gravity from Smith and Sandwell, 1995.)

previously suggested by many others (e.g., Hyndman and Ellis, 1981; Berube *et al.*, 1989; Rohr *et al.*, 2000; Lay *et al.*, 2013).

This strain partitioning is consistent with model predictions for an angle of convergence $> 20^\circ$, as summarized in the Introduction section. We note the depth of the QCT decreases from south to north along the southern segment, consistent with progressive thickening of the terrace with time. Seismic refraction studies show that velocities corresponding to upper oceanic crust occur at depths of a few kilometers beneath the southern segment of the QCT (Horn *et al.*, 1984; Dehler and Clowes, 1988; Spence and Long, 1995), suggesting that at least the upper oceanic crust is involved in shortening of the Pacific plate southwest of the QCF.

Between 53.2° and 55.4° N, which we call the central section of QCT, a linear scarp-bounded terrace is not present; instead, this section is characterized by ridges and basins that are oblique to the main fault trace (Fig. 2b). Ridges trend both northwest–southeast and north–south. This change in morphology is also reflected in the gravity anomalies, which also show an en echelon pattern of relative highs and lows (Fig. 5b). The pattern of complicated topography and multiple oblique structural zones appears to continue to the north until about 56° N. The central section of the QCT is also wider and deeper than near 53° N.

North of 55.4° N (the northern QCT section), multiple structural zones defined by ridges and basins in the Pacific plate appear to coalesce into a single fault strand, and the QCF is again characterized by a linear terrace (Bruns and Carlson, 1987). The topographic terrace of the northern QCT segment may be related to increased sediment input from the continent as indicated by the Baranoff Fan (Fig. 2), which is thought to have initiated approximately 7 Ma in the wake of the Yakutat block (Walton *et al.*, 2014) that collided with North America approximately 10 Ma (Gulick *et al.*, 2007). This collision may also have reactivated splay faults from the QCF that extend into the North America plate. The southernmost of these faults is the Chatham Strait fault (CSF in Fig. 2a), which may have been active during the Craig earthquake sequence (Roland *et al.*, 2014) and may represent the southern extension of the Denali fault.

The primary objective of this article is to explain the change in seafloor morphology, upper crustal structure, and earthquake mechanisms from the southern to the central QCT segments in the context of models for transpression along plate boundaries.

The along-strike distance over which the complicated morphology of the central segment is observed (roughly 250 km north of 53.2° N; Fig. 2b) is similar to the predicted

amount of displacement along the QCF since the initiation of oblique convergence at 5–6 Ma, consistent with the inference that this morphology is a consequence of the change in plate motion and the bend in the fault.

Multichannel Seismic Reflection Data

Acquisition and Processing

Seismic lines that cross the central segment of the area are shown in Figure 6, displayed from north to south and aligned along the QCF. Multichannel seismic reflection data were collected by the R/V *Maurice Ewing* along and across the QCF and adjacent terrace west of Dixon entrance as part of the ACCRETE project (Hollister and Andronicos, 1997). The locations of seismic lines acquired during cruise EW9412 (solid lines labeled EW1250–EW1265 in Fig. 5) were designed to complement a 1977 seismic reflection data set collected by the U.S. Geological Survey on the R/V *S.P. Lee* (Snively *et al.*, 1981; dashed track lines labeled USGS1–USGS5 in Fig. 5). The location of a seismic line discussed by Bruns and Carlson (1987) is also shown (BC951 in Fig. 5). BC951 is the southernmost line in a 1978 survey of the Queen Charlotte/Fairweather fault that extended north to the Gulf of Alaska.

Processing details for the EW9412 data are given by Scheidhauer (1997) and Scheidhauer *et al.* (1999) and included sorting into 60-fold data with a common midpoint spacing of 12.5 m, band-pass filtering (10–60 Hz), velocity analysis at 1.25 km intervals, stacking, finite-difference migration, and depth conversion. An example of stacking velocities for line 1262 is shown in Figure 7. A velocity model derived from the stacking velocities and from prior seismic refraction experiments in the region was used for migration and depth conversion. Total source volume was 138 L (8400 in³). Because of the very strong seafloor multiples resulting from a reflection coefficient of ~0.5 along most of the profiles (Scheidhauer, 1997), the first multiple and underlying data were muted prior to migration. The R/V *Lee* data (see Data and Resources) were 24-fold with a common midpoint spacing of 50 m, and total source volume was 22 L (1326 in³) (Snively *et al.*, 1981; Rohr *et al.*, 1992). The R/V *Lee* data were migrated using a frequency–wavenumber algorithm and a velocity of 1500 m/s for this publication. The migrated R/V *Lee* data in Figure 6 and the depth-converted data in Figures 8–10 have not been previously published.

Constraints on Timing

Timing of the deformation imaged in these seismic lines is uncertain because of the absence of any deep drill holes in this region and the lack of correlatable reflections across the faults bounding the terrace. Deformation must be younger than about 15 Ma, the age of the underlying oceanic crust. The Miocene–Pliocene unconformity (5.3 Ma), labeled U in Figures 8 and 9, can be tentatively identified west of the terrace based on an abrupt change in seismic interval velocity

and the presence of truncated or bright reflectors (Snively *et al.*, 1981; Scheidhauer, 1997; Walton *et al.*, 2015). This unconformity is regionally observed and may be associated with a period of erosion or nondeposition coinciding with the onset of transpression at 5–6 Ma.

Beneath the terrace, where velocities in the upper kilometers are higher than in the trough (Fig. 7), we are unable to identify any temporal stratigraphic markers. We expect that sediments of a given age will have a higher velocity beneath the terrace than beneath the abyssal plain because of deformation-induced dewatering. Because of high Pleistocene sedimentation rates, most of the sediment imaged beneath the terrace may be quite recent and likely also postdates 5–6 Ma.

Structural Observations and Interpretations

The structure of the QCF system varies along strike from a half-graben on the North American side of the plate accompanied by a seafloor step on lines EW1262 and USGS5 (Fig. 6 of this article and figs. 8–10 of Rohr *et al.*, 2000), indicative of a local extensional stepover, to an apparent pop-up structure on line EW1250, where there is a compressional stepover in the fault (fig. 12 in Rohr *et al.*, 2000). Rohr *et al.* (2000) concluded that the QCF is a throughgoing vertical boundary between the Pacific and North America plates based on apparent decoupling of glacial rebound in the North American plate from the Pacific plate. However, it was not possible to rule out a shallow strike-slip fault above underthrust Pacific plate crust based on seismic-reflection data, seismicity, and modeling of gravity data along seismic line EW1262 (e.g., fig. 15 in Rohr *et al.*, 2000). Similarly, seismic refraction data across the southern segment cannot resolve the amount of underthrusting of Pacific plate crust beneath the QCF, although receiver functions from sites on northern Haida Gwaii suggest that subducted Pacific plate crust may extend at least as far east as Graham Island (Bustin *et al.*, 2007).

Line EW1262 is shown at larger scale in Figure 8, with the two-way travel time axis converted to depth beneath the sea surface using interval velocities derived from smoothed stacking velocities (Scheidhauer, 1997; Scheidhauer *et al.*, 1999). Line BC951 (Bruns and Carlson, 1987), 30 km to the north, and USGS5, 10 km to the south, show similar features. All three lines cross a narrow, north–south-oriented topographic ridge at the western edge of the terrace that separates the undeformed, eastward-thickening sedimentary strata of the Queen Charlotte Trough from the folded strata that lie between this outer ridge and the QCF (fault zone A in Figs. 6, 8, and 9). Internal structure is poorly resolved within the ridge, which we interpret to be a flower structure associated with a strike-slip fault in a transpressional zone (e.g., Sylvester, 1988). This structure is influencing, and is influenced by, seafloor sedimentation and erosion (Walton *et al.*, 2014), as the ridge formed by fault zone A deflects the northern branch of the Mukluk channel to the south and the channel erodes the eastern flank of the ridge. These processes are indicated by high seafloor reflectivity and the intersection of shallow

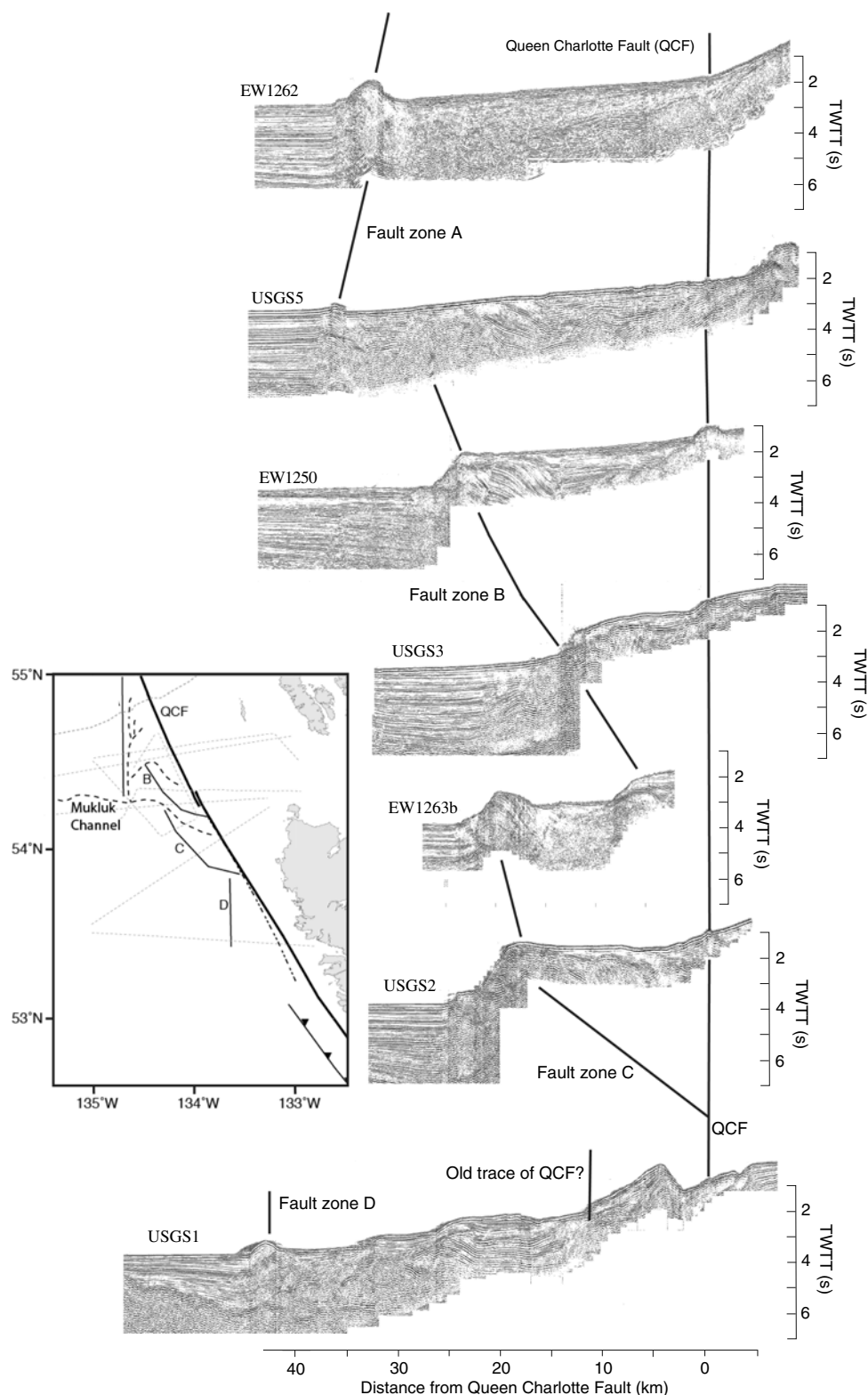


Figure 6. Stacked and migrated multichannel seismic sections aligned along the QCF. See Figure 5b for locations of the data shown here. For the EW9412 lines (Scheidhauer *et al.*, 1999; Rohr *et al.*, 2000), smoothed interval velocities derived from stack velocities were used for migration. Because no velocity information was available for the USGS profiles, these were migrated using a constant velocity appropriate for the water column, which adequately corrects for the effects of rough seafloor and very shallow subsurface structure but is not adequate to image deeper structural details. The inset shows the location in map view of the primary structures identified on the seismic reflection sections; light gray dotted lines show locations of seismic lines. Black dotted lines indicate the location of the southern branch of the Mukluk channel (from Bruns *et al.*, 1992). Black dotted-dashed line is a possible prior trace of the QCF.

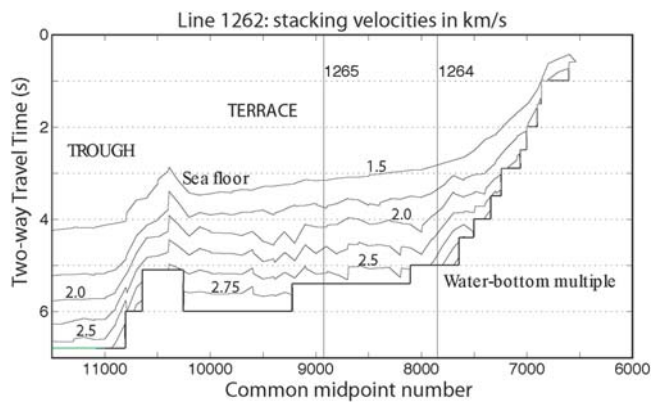


Figure 7. Stacking velocities for EW1262 shown as contours as a function of location along the line and two-way travel time (twtt). Stacking velocities for all east–west lines are given by Scheidhauer *et al.* (1999).

reflections with the seafloor immediately east of the topographic ridge created by this fault (Fig. 8, inset).

Between fault zone A and the QCF, the QCT is marked by folded strata overlying a region of incoherent reflectivity interpreted as an accretionary mélangé (Rohr *et al.*, 2000), and the top of the basement (assumed to be oceanic crust of the Pacific plate) is not imaged (Fig. 8). The intensity of folding decreases upward, indicating that folding was active during deposition. Folding also decreases to the east, an observation noted earlier by Bruns and Carlson (1987), who interpreted an inner and outer structural zone along the QCF north of our study area. Active folding that continues to the present time is imaged between fault zone A and 33 km (i.e., within the outer structural zone shown in Fig. 8). In contrast, the region from 33 km to the QCF (the inner structural zone in Fig. 8)

has undergone recent tilting but little internal folding. A similar pattern of buried folds beneath the terrace is observed on line EW1265 (Scheidhauer *et al.*, 1999). Folds trending oblique to major strike-slip faults are observed in other transpressional settings (e.g., Titus *et al.*, 2007), and we similarly interpret them as recording a combination of wrench and contractional deformation. We note that although Bruns and Carlson (1987) extended their identification of an inner and outer structural zone as far north as 57.5° N, the distance between the outer structural zone and the QCF is approximately constant and defines a relatively simple, 20–25 km wide terrace on all seismic profiles that cross the QCF north of 56° N, in contrast to the wide zone of complex morphology and structure characteristic of the central segment (53.2° – 55.2° N).

Fault zone A extends to the south and intersects line EW1263a obliquely (Fig. 6, inset). On line EW1263a (Fig. 9), fault zone A has no topographic manifestation, but an offset of ~ 750 m is observed at a depth of ~ 5.5 km. At shallower depths, folding is observed with a reduced amplitude of ~ 550 m at a depth of 3.3 km and ~ 275 m at a depth of 2.6 km, indicating deformation over a significant period of time. Near the seafloor above fault zone A, reflections are discontinuous, indicative of seafloor erosion in the Mukluk channel, in contrast to farther north along this line, where reflections are continuous. The horizontal extent of seafloor erosion is suggested by faint migration artifacts likely resulting from small (relative to the quarter-wavelength of the dominant energy in the seismic data, which is 6 m) topographic steps on the seafloor. Fault zone A is parallel to the magnetic anomaly trend (Fig. 2a), and we infer that a normal fault formed at the spreading center has been reactivated as a secondary shear fault oblique to the main strand of the QCF. Because the basement offset associated with fault

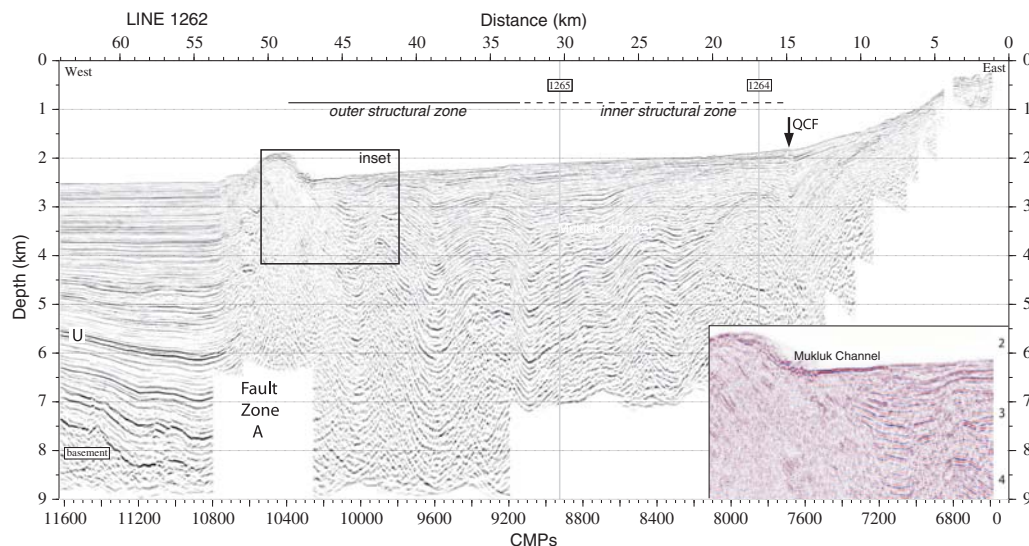


Figure 8. Time-to-depth conversion of a portion of EW1262 showing the QCF, fault zone A, and the inner and outer structural zones. Distance along the profile is shown along the top of the display, and common mid-point (CMPs) corresponding to the archived data are shown along the bottom. The intersections with EW1264 and EW1265 are also shown. U is a regional unconformity interpreted to have an age of 5.3 million years. See text for additional discussion.

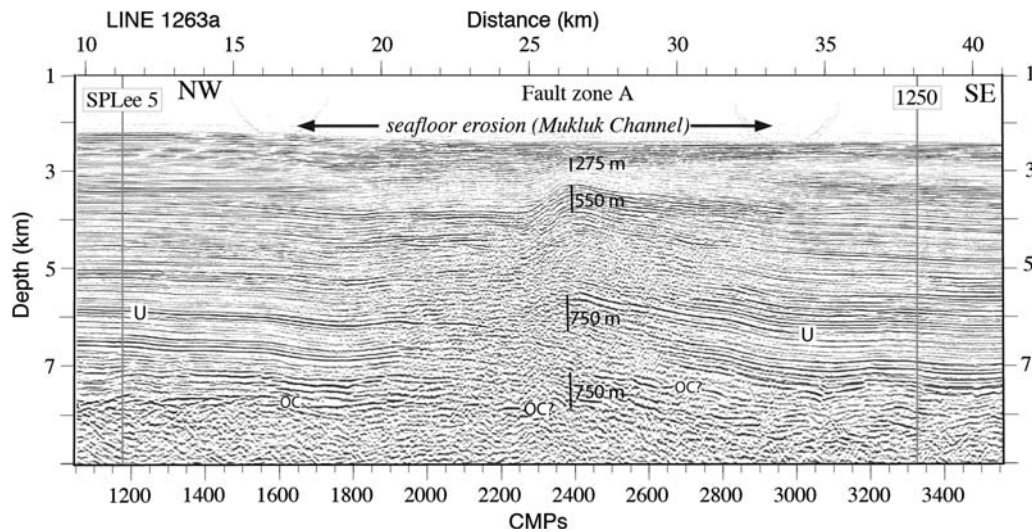


Figure 9. Time-to-depth conversion of a portion of EW1263a showing the buried southern extension of fault zone A. Distance along the profile is shown along the top of the display, and CMPs corresponding to the archived data are shown along the bottom. Offset on fault zone A is shown at several different depths. U identifies a regional unconformity interpreted to have an age of 5.3 Ma. See text for additional discussion.

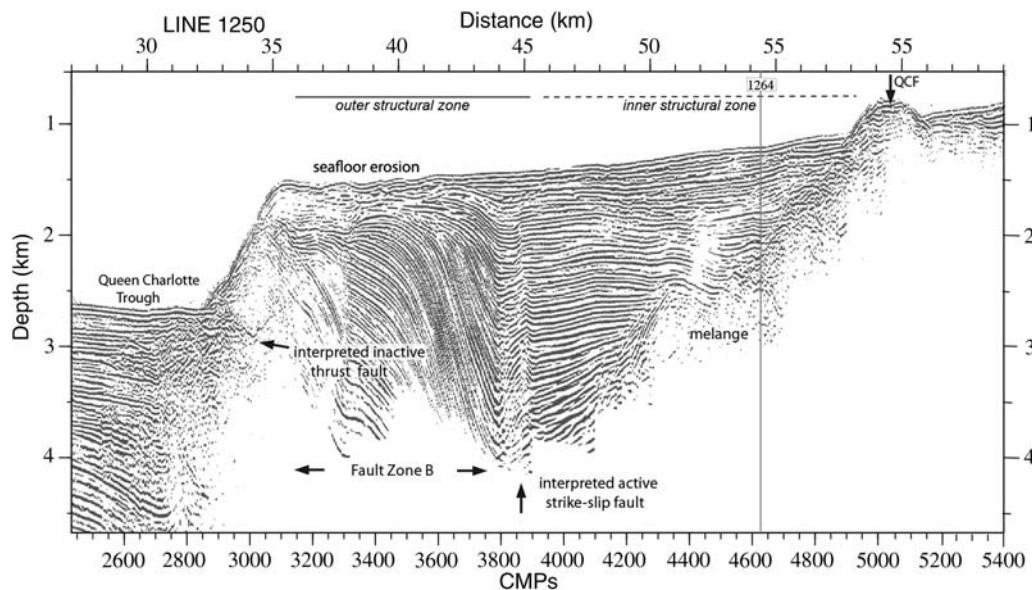


Figure 10. Time-to-depth conversion of a portion of EW1250. Distance along the profile is shown along the top of the display, and CMPs corresponding to the archived data are shown along the bottom. See text for additional discussion.

zone A is similar to the amplitude of folding of the Miocene/Pliocene unconformity (U in Fig. 9), most of the motion recorded in these sediments has taken place since that time. This interpretation is consistent with deformation on fault zone A being initiated as the Pacific plate adjacent to the QCF moved past the bend in the QCF, resulting in a decrease in the angle of oblique convergence below 15° .

On line EW1250, the terrace is narrower and shallower than on line EW1262 (Fig. 10), and its seaward edge is marked by a steep scarp, east of which is a thick, landward-

dipping wedge that shows sharp kinks suggestive of syntectonic deposition above a blind-thrust fault (Shaw and Suppe, 1994). As on line EW1262, strata cannot be correlated across this scarp. At the base of the scarp, a reflection is observed that may be a low-angle thrust similar to that seen at the deformation front of the northern Cascadia subduction zone (e.g., Davis and Hyndman, 1989), supporting the inference of thrust and reverse faulting parallel to the QCF. The abrupt truncation of reflections beneath the westernmost part of the terrace and the presence of steeply dipping discontinuities in

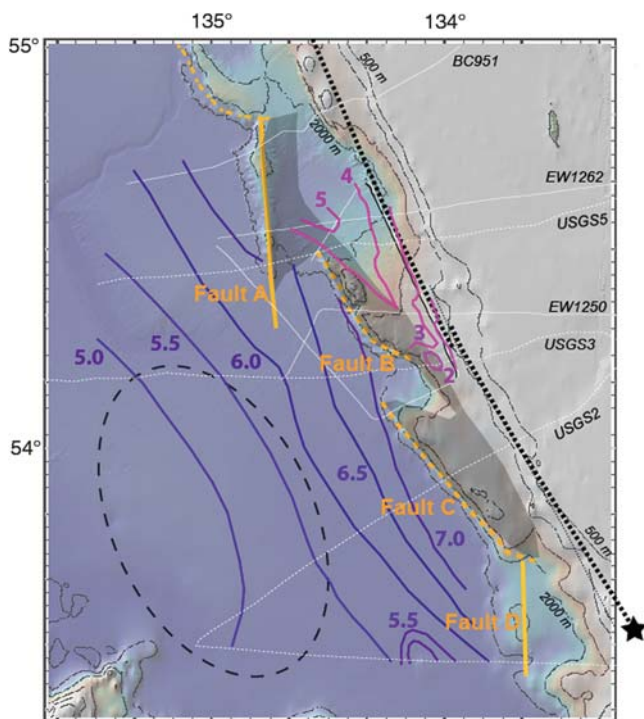


Figure 11. Summary of our structural interpretation overlain on bathymetry (see box in Fig. 5a for location). Solid orange lines show the locations of fault zones A and D interpreted from the seismic data. Dashed orange lines show the interpreted relict thrust faults related to reactivated strike-slip fault zones B and C. Gray shading delimits the outer structural zone characterized by a considerable folding and faulting. Violet contours are the depth in twtt in seconds to the top of the oceanic crust of the Pacific plate and show the deepening of the oceanic crust toward the QCT and the offset in the oceanic crust associated with the southern tip of fault zone A. Pink contours are the twtt (s) to the top of mélangé beneath the terrace and show a northward-thickening basin within the QCT between lines EW1250 and EW1262. The dashed oval shows the region of buried extensional faults discussed by Walton *et al.* (2015). Bathymetric contours are at 500 m intervals. Swath bathymetry is only available in the northwestern part of the region shown in this map.

reflectivity suggest later deformation of an accreted sediment wedge by strike-slip faulting. The seafloor overlying fault zone B is erosional, and the ridge associated with fault zone B is breached (Fig. 10), in another example of the interaction between tectonics and seafloor channel development.

Bathymetric continuity suggests that the outer ridge and narrow terrace imaged on USGS3 (Fig. 6) are also manifestations of fault zone B, which is oriented $\sim 15^\circ$ counterclockwise to the primary trace of the QCF (Fig. 11). The strike of fault zone B is similar to the strike of the southern segment of the QCT and curves to the east to merge with the QCF. We infer that fault zone B merges at depth with a thrust fault that was formed parallel to the QCF south of 53.2° N and has been reactivated to accommodate secondary, primarily strike-slip, deformation oblique to the QCF. CMT solutions for earthquakes along this segment of the fault, including one event that may have occurred on fault zone B, are all strike slip.

Interaction at depth between pre-existing thrust faults and later-stage strike-slip faults is not well imaged. Similar structures are observed on lines EW1263b and USGS2, defining fault zone C (Fig. 6).

Eight kilometers south of USGS2, USGS1 crosses a north-south-trending ridge similar to the ridge that characterizes fault zone A; we call this fault zone D in Figures 5 and 11. Between the QCF and fault zone D, deformation is greater beneath the western part of the terrace, e.g., on lines EW1262 and USGS5. This line also shows an unusual uplifted and tilted fault-bound block west of the QCF (Fig. 6) that extends from 53.2° to 53.8° N (Fig. 5a). We speculate the western boundary of the block is an earlier trace of the QCF and that the block was formed by an eastward jump and reorientation of the QCF. Alternatively, it may represent another strand of the QCF, contemporaneous with the primary trace of the QCF. GLORIA data are of limited use in evaluating the history of this feature because it falls within the nadir of a GLORIA swath (i.e., along the ship's track). If the primary trace of the QCF has jumped east, then the bend in the fault at 53.2° N would have been significantly more pronounced in the past, as shown by the dotted line in Figure 2b. Additional data are needed to investigate this hypothesis.

Discussion

The central segment of the QCF (53.2° – 55.4° N) has a complicated morphology that can be correlated with the relative plate motion history, recent earthquake activity, and subsurface structure imaged using seismic reflection techniques. Our observations and interpretations, which are summarized in map view in Figure 11 and shown schematically in Figure 12, suggest an abrupt change in how transpressional deformation resulting from Pacific/North America plate motion is accommodated as the angle of oblique convergence decreases.

From 52° – 53.2° N (southern QCT), where the angle of oblique convergence is greater than 15° , the terrace is linear and parallel to the strike of the QCF (Fig. 12). The topography, crustal structure, and seismic activity, including the 2012 Haida Gwaii low-angle thrust fault and several smaller thrust events in the past two decades, all suggest that the QCT adjacent to this segment of the QCF is constructed by folding and thrust faulting of sediments, and possibly crust, of the Pacific plate along northeast-dipping faults that strike parallel to the QCF. Similar partitioning of deformation into strike-slip motion on a near-vertical fault and shortening on thrust faults (or a single thrust fault) oriented approximately parallel to this strike-slip fault has been documented in a number of places (e.g., Mount and Suppe, 1987, 1992; Tikoff and Teyssier, 1994; Walcott, 1997; Miller, 1998; Titus *et al.*, 2011; Lay *et al.*, 2013). Although seismic refraction data suggest the upper oceanic crust is involved in this process (Horn *et al.*, 1984; Dehler and Clowes, 1988), a recent receiver function study (Bustin *et al.*, 2007) suggests that the oceanic crust of the Pacific plate is at least partially subducted beneath the Graham Island

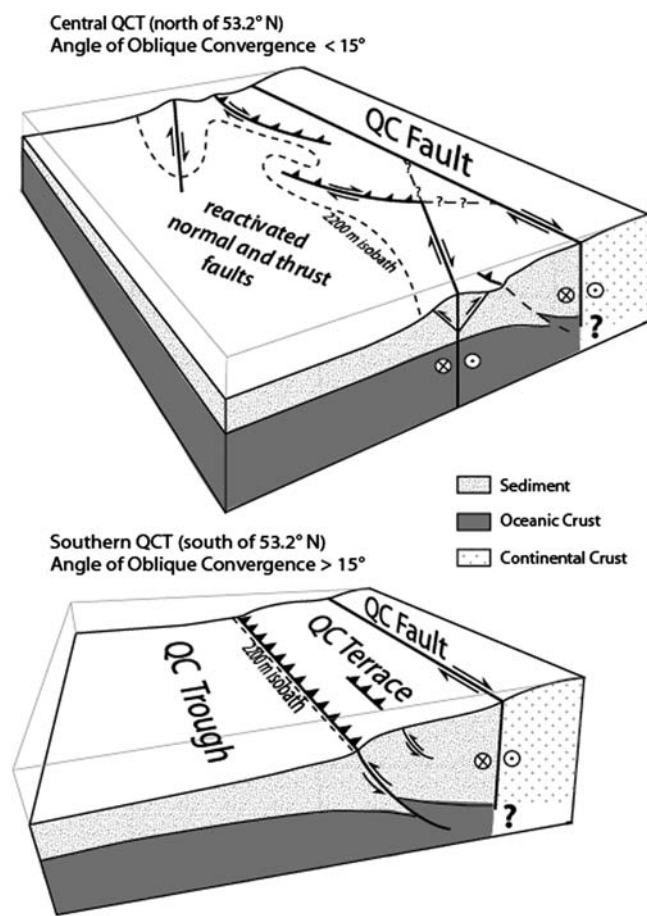


Figure 12. Schematic illustration of the contrasting deformation regimes as the angle of compression decreases from $>15^\circ$ to $<15^\circ$.

near 53° N. The large number of normal-faulting earthquakes that followed the Haida Gwaii event also suggests bending of the Pacific plate in response to loading resulting from compressional faulting within the terrace, although a quantitative analysis of the load required to cause the observed flexure and faulting of the Pacific plate beneath the Queen Charlotte Trough or the stresses needed to trigger the normal faulting are beyond the scope of this study.

Between 53.2° and 54.4° N (central QCT), where the angle the plate motion vector makes with the QCF decreases from $>15^\circ$ to $\sim 5^\circ$, the seafloor morphology and structural geometry are quite different (Figs. 11, 12). Terrace morphology is characterized by a complex pattern of ridges and deformed basins that are oblique to the main strand of the QCF. We have identified two distinctive fault types along this segment. Fault zones A and D are subvertical, oriented $\sim 25^\circ$ clockwise (155° counterclockwise) to the QCF and are inferred to be wrench faults, both of which accommodate primarily horizontal motion; a component of shortening across them results in the formation of classic flower structures. The total amount of displacement on these faults is poorly constrained but appears to decrease in magnitude with distance

from the QCF. Because they are parallel to magnetic anomalies generated by seafloor spreading, we interpret them to indicate reactivation by strike-slip faulting of normal faults that formed at a spreading center.

Fault zones B and C have a very different appearance and orientation ($\sim 15^\circ$ counterclockwise) in seismic reflection data. The seaward edge of the terrace associated with these structures resembles the frontal thrust of an accretionary wedge that is being cut by steeply dipping thrust and strike-slip faults. Although they are now oblique to the QCF, their orientation is similar to that of the thrust faults parallel to the QCF that are building the QCT south of 53.2° N. The region between these faults and the QCF is characterized by deformed basins that plunge to the north, with deformation focused on the west side of the basins. We interpret these faults to represent partial dismemberment of the terrace formed south of 53.2° N by strike-slip faults that may sole at depth into pre-existing thrust faults.

These observations lead us to ask what causes such an abrupt difference in structural geometry along strike of the QCF. Our results are remarkably consistent with analytical, numerical, and analog studies of transpression summarized in the Introduction section. There are slight variations, however, between the theoretical predictions and deformation along the QCF. The predicted transition from a pure shear to a simple shear-dominated transpressive regime occurs abruptly at the relatively small angle of 15° rather than at the predicted 20° (Fossen and Tikoff, 1993). Transpression (in the strict definition of Sanderson and Marchini, 1984) lies on a continuum with other types of deformation that could result from oblique convergence (Fossen and Tikoff, 1998). In particular, any along-strike component of elongation will lower the angle of convergence at which the change in behavior occurs. Because the documented deformation occurs on the outward (western) margin of the curved QCF system, there is likely a component of fault-parallel elongation of the material west of the fault.

We also ask why the deformation that we observe appears to be focused on the oceanic lithosphere on the western side of the QCF in this region, even though the plates on both sides of the QCF are young, thin, and hot (Rohr et al., 2000). We hypothesize that the deformation associated with the QCF, as imaged on seismic profiles, is focused in a narrow zone within the Pacific plate because of the presence of pre-existing zones of weakness in the oceanic lithosphere that have orientations similar to the orientations predicted for secondary shears in a slightly transpressive strike-slip fault system in a homogeneous medium (e.g., Tschalenko, 1970; Sanderson and Marchini, 1984; Tikoff and Teyssier, 1994; Walcott, 1997). These zones of weakness in the oceanic lithosphere result from spreading ridge-related normal faults and from thrust faults created when the lithosphere was farther south in the regime where compression is accommodated by thrust faults parallel to the QCF.

We briefly consider three alternative models for the along-strike change in terrace morphology. First, we con-

sider whether the change in morphology could result purely from geomorphic forces that differ between the segment of the QCF that is flanked on the east by the Haida Gwaii and that which is flanked on the east by Dixon entrance. Could the lower elevation of Dixon entrance and smaller amount of compression of the terrace north of 53.2° N lead to meandering of the Mukluk channel, thus cutting the terrace into the observed oblique ridges? Because the seismic reflection data indicate the ridges around which the channel meanders are cored by active faults, we consider this mechanism to be unlikely. Second, we consider whether the change in tectonic response to transpression occurs because of the increasing age and strength of the plate rather than because of the change in the orientation of the QCF. We reject this hypothesis because the change in age is gradual and the change in morphology is abrupt and coincident with the change in angle. Third, we consider the argument of Chéry *et al.* (2001), based on observations of the San Andreas fault system, that the strength of the primary strike-slip fault is the dominant factor controlling how the convergent component of plate motion is accommodated. We consider this hypothesis to be unlikely because there is no independent evidence for an abrupt change in the strength of the QCF at 53.2° N and note that aftershocks of the 1949 earthquake may have extended south of this latitude.

Finally, we consider a broader view of regional deformation, which suggests that deformation in both plates (Horn *et al.*, 1984; Rohr *et al.*, 2000) contributes to the total shortening implied by the MORVEL plate motion vectors (Fig. 1). Microseismicity across Graham Island (Berube *et al.*, 1989) and removal of as much as 1700 m of Miocene–Pliocene sediments on Graham Island (Vellutini and Bustin, 1991) attest to active uplift in Haida Gwaii, and Miocene extensional faults have been reactivated to accommodate shortening across Hecate strait (Rohr *et al.*, 2000). A complete inventory of shortening in the North American and Pacific plates distributed over the entire width of the deforming plate boundary is beyond the scope of this article.

Conclusions

We have documented along-strike changes in the structure and morphology of the Pacific plate adjacent to the QCF that are correlated with changes in the angle of oblique convergence across the fault predicted by the MORVEL global plate motion model. Where the angle of oblique convergence is greater than 15°, both strike-slip and reverse-fault motions occur, with shortening accommodated by thrust and reverse faults that strike at a low angle to the main strike-slip fault and have a range of dips. This geometry results in the formation of a well-defined linear submarine terrace on the Pacific plate adjacent to the QCF that gets shallower to the north with continuing deformation. When the angle of oblique convergence is less than 5° (north of our study area), seafloor morphology indicates that deformation is localized within a narrow zone. When the angle of compression is 5°–15°, how-

ever, distinct synthetic strike-slip faults are observed and result in a broad zone of complex morphology. The orientation of the splay faults suggests reactivation of normal faults formed near the spreading ridge and thrust faults formed farther south, where the angle of oblique convergence in transpression was greater than 15°. This type of behavior is consistent with analog and numerical models of transpression. Although similar patterns have been documented along other transpressive plate boundaries, it is perhaps particularly evident along the QCF system because of (1) the relatively simple structure of oceanic crust, (2) the presence of structures in the Pacific plate that are optimally oriented for reactivation as synthetic shear faults oblique to the QCF, and (3) the presence of a marine sedimentary record of Miocene and later deformation in the sediments overlying the Pacific plate crust to record the deformation history.

Data and Resources

Earthquake mechanisms were downloaded from the Global Centroid Moment Tensor (CMT) catalog (<http://www.globalcmt.org/CMTsearch.html>; last accessed 21 May 2014). Plate motion vectors were calculated using the MORVEL plate motion calculator at <http://geoscience.wisc.edu/~chuck/MORVEL/> (last accessed 4 April 2014). Bathymetry from the global multiresolution topography (GMRT) database accessed via GeoMapApp on 23 April 2014. Data from the both R/V *Lee* surveys are available from the U.S. Geological Survey (USGS) National Archive of Marine Surveys (<http://walrus.wr.usgs.gov/NAMSS>; last accessed February 2015). The unprocessed EW9412 data are available from the Academic Seismic Portal at Lamont-Doherty Earth Observatory (<http://www.marine-geo.org/portals/seismic>; last accessed February 2015); stacked and migrated sections can also be obtained in SEG-Y format from the Academic Seismic Portal at the University of Texas Institute for Geophysics (UTIG; www.ig.utexas.edu/sdc, last accessed February 2015).

Acknowledgments

This manuscript represents an update, triggered by the recent earthquakes, of an unpublished manuscript originally prepared over a decade ago based on M. Scheidhauer's MS thesis at Oregon State University. We thank John Diebold, Captain Ian Young, and the crew of the R/V *Ewing* for their efforts in data acquisition during cruise EW9412. We thank Lincoln Hollister for allowing us to extend the ACCRETE survey across the Queen Charlotte fault following Rohr's experiment design. Support for data analysis from cruise EW9412 was provided by National Science Foundation (NSF) Grants EAR-9219870 and EAR-9527011 to Oregon State University. Maps were constructed using Generic Mapping Tools (GMT) (Wessel and Smith, 1995). We thank University of Wisconsin undergraduate student Melly Meyer for drafting Figure 12 and Guest Editor Peter Haeussler, Reviewer Tom Pratt, and an anonymous reviewer for constructive comments that improved the clarity of the text and figures. This is University of Texas Institute for Geophysics (UTIG) Contribution Number 2730.

References

- Atwater, T. (1989). Plate tectonic history of the northeast Pacific and western North America, in *The Eastern Pacific Ocean and Hawaii*, E. L. Winterer, D. M. Hussong, and R. W. Decker (Editors), The Geology of North America, Boulder, Colorado, 21–72.
- Atwater, T., and J. Stock (1998). Pacific-North America plate tectonics of the Neogene southwestern United States; an update, *Int. Geol. Rev.* **40**, 375–402.
- Berube, J., G. C. Rogers, R. M. Ellisand, and E. O. Hasselgren (1989). A microseismicity study of the Queen Charlotte Island region, *Can. J. Earth Sci.* **26**, 2556–2566.
- Bostwick, T. K. (1984). A re-examination of the August 22, 1949 Queen Charlotte earthquake, *M.S. Thesis*, University of British Columbia.
- Braun, J., and C. Beaumont (1995). Three-dimensional numerical experiments of strain partitioning at oblique plate boundaries: Implications for contrasting tectonic styles in the southern Coast Ranges, CA, and central South Island, NZ, *J. Geophys. Res.* **100**, 18,059–18,074.
- Braunmiller, J., and J. L. Nabelek (2002). Seismotectonics of the Explorer region, *J. Geophys. Res.* **107**, doi: [10.1029/2001JB000220](https://doi.org/10.1029/2001JB000220).
- Bruns, T. R., and P. R. Carlson (1987). Geology and petroleum potential of the southeast Alaska continental margin, *Earth Sci. Series* **6**, 269–282.
- Bruns, T. R., A. J. Stevenson, and M. R. Dobson (1992). GLORIA investigation of the Exclusive Economic Zone in the Gulf of Alaska and off southeast Alaska: M/V Farnella Cruise F7-89-GA, June 14–July 13, 1989, *U.S. Geol. Surv. Open-File Rept.* 92-317, 16 pp.
- Burbridge, D. R., and J. Braun (1998). Analogue models of obliquely convergent continental plate boundaries, *J. Geophys. Res.* **103**, 15,221–15,237.
- Bustin, A. M. M., R. D. Hyndman, H. Kao, and J. F. Cassidy (2007). Evidence for underthrusting beneath the Queen Charlotte margin, British Columbia, from teleseismic receiver function analysis, *Geophys. J. Int.* **171**, 1198–1211.
- Casas, A. M., D. Gapais, T. Nalpas, K. Besnard, and T. Romàn-Berdiel (2001). Analog models of transpressive systems, *J. Struct. Geol.* **23**, 733–743.
- Chase, R. L., and D. L. Tiffin (1972). Queen Charlotte Fault-Zone, British Columbia; in *Marine Geology and Geophysics*, in *Proceedings of 24th International Geological Congress*, J. E. Gill, J. Béland, and E. W. Mountjoy (Editors), Montreal, Quebec, Canada, Sec. 8, 17–28.
- Chéry, J., M. D. Zoback, and R. Hassani (2001). An integrated mechanical model of the San Andreas fault in central and northern California, *J. Geophys. Res.* **106**, 22,051–22,066.
- Christensen, D. H., and L. J. Ruff (1988). Seismic coupling and outer rise earthquakes, *J. Geophys. Res.* **93**, 13,421–13,444, doi: [10.1029/JB093iB11p13421](https://doi.org/10.1029/JB093iB11p13421).
- Cox, A., and D. Engebretson (1985). Change in motion of Pacific plate 5 Myr BP, *Nature* **313**, 472–474.
- Davis, E. E., and R. D. Hyndman (1989). Accretion and recent deformation of sediments along the northern Cascadia subduction zone, *Geol. Soc. Am. Bull.* **101**, 1465–1480.
- Dehler, S. A., and R. M. Clowes (1988). The Queen Charlotte Islands refraction project, part I, The Queen Charlotte Fault Zone, *Can. J. Earth Sci.* **25**, 1857–1870.
- DeMets, C., R. G. Gordon, and D. F. Argus (2010). Geologically current plate motions, *Geophys. J. Int.* **181**, 1–80, doi: [10.1111/j.1365-246X.2009.04491.x](https://doi.org/10.1111/j.1365-246X.2009.04491.x).
- DeMets, C., R. G. Gordon, D. F. Argus, and S. Stein (1994). Effect of recent revisions to the geomagnetic reversal time scale on estimates of current plate motions, *Geophys. Res. Lett.* **21**, 2191–2194.
- Doser, D. I., and H. Rodriguez (2011). A seismotectonic study of the southeastern Alaska region, *Tectonophysics* **497**, 105–113.
- Dobrovine, P. V., and J. A. Tarduno (2008). A revised kinematic model for the relative motion between Pacific oceanic plates and North America since the Late Cretaceous, *J. Geophys. Res.* **113**, doi: [10.1029/2008JB005585](https://doi.org/10.1029/2008JB005585).
- Ekström, G., M. Nettles, and A. M. Dziewonski (2012). The global CMT project 2004–2010: Centroid-moment tensors for 13,017 earthquakes, *Phys. Earth Planet. In.* **200**, 1–9, doi: [10.1016/j.pepi.2012.04.002](https://doi.org/10.1016/j.pepi.2012.04.002).
- Fossen, H., and B. Tikoff (1993). The deformation matrix for simultaneous simple shearing, pure shearing, and volume change, and its application to transpressional/transensional tectonics, *J. Struct. Geol.* **15**, 413–422.
- Fossen, H., and B. Tikoff (1998). Extended models of transpression and transension, and application to tectonic settings, in *Continental Transpressional and Transensional Tectonics*, R. E. Holdsworth, R. A. Strachan, and J. F. Dewey (Editors), Geol. Soc. London, Sp. Publ., London, 135, 15–33.
- Fossen, H., B. Tikoff, and C. Teyssier (1994). Strain modeling of transpressional and transensional deformation, *Norsk Geologisk Tidsskrift* **74**, 134–145.
- Gulick, S. P. S., L. A. Lowe, T. L. Pavlis, J. V. Gardner, and L. A. Mayer (2007). Geophysical insights into the Transition fault debate: Propagating strike slip in response to stalling Yakutat block subduction in the Gulf of Alaska, *Geology* **35**, 763–766.
- Hollister, L. S., and C. L. Andronicos (1997). A candidate for the Baja British Columbia fault system in the Coast Plutonic complex, *GSA Today* **7**, 1–17.
- Horn, J. R., R. M. Clowes, R. M. Ellis, and D. N. Bird (1984). The seismic structure across an active oceanic/continental transform fault zone, *J. Geophys. Res.* **89**, 3107–3120.
- Hyndman, R. D., and R. M. Ellis (1981). Queen Charlotte fault zone: Micro-earthquakes from a temporary array of land stations and ocean bottom seismographs, *Can. J. Earth Sci.* **18**, 776–788.
- Hyndman, R. D., and T. S. Hamilton (1993). Queen Charlotte area Cenozoic tectonics and volcanism and their association with relative plate motions along the Northeastern Pacific margin, *J. Geophys. Res.* **98**, 14,257–14,277.
- Lay, T., C. J. Ammon, H. Kanamori, M. J. Kim, and L. Xue (2011). Outer trench-slope faulting and the 2011 M_w 9.0 of the Pacific coast of Tohoku earthquake, *Earth Planets Space* **63**, 713–718.
- Lay, T., L. Ye, H. Kanamori, Y. Yamazaki, K. F. Cheung, K. Kwong, and K. D. Koper (2013). The October 28, 2012 M_w 7.8 Haida Gwaii underthrusting earthquake and tsunami: Slip partitioning along the Queen Charlotte Fault transpressional plate boundary, *Earth Planet. Sci. Lett.* **375**, 57–70.
- Leonard, M. (2010). Earthquake fault scaling: Self-consistent relating of rupture length, width, average displacement, and moment release, *Bull. Seismol. Soc. Am.* **100**, 1971–1988.
- Lewis, P. D., J. W. Haggart, R. G. Anderson, C. J. Hickson, T. I. Thompson, J. R. Dietrich, and K. M. M. Rohr (1991). Triassic to Neogene geologic evolution of the Queen Charlotte region, *Can. J. Earth Sci.* **28**, 854–869.
- Mackie, D. J., R. M. Clowes, S. A. Dehler, R. Ellis, and P. Morel A-l’Huissier (1989). The Queen Charlotte Islands refraction project. Part II. Structural model for transition from Pacific plate to North American plate, *Can. J. Earth Sci.* **26**, 1713–1725, doi: [10.1139/e89-146](https://doi.org/10.1139/e89-146).
- McCaffrey, R. (1992). Oblique plate convergence, slip vectors, and forearc deformation, *J. Geophys. Res.* **97**, 8905–8915.
- Miller, D. D. (1998). Distributed shear, rotation, and partitioned strain along the San Andreas fault, central California, *Geology* **26**, 867–870.
- Mount, V. S., and J. Suppe (1987). State of stress near the San Andreas fault: Implications for wrench tectonics, *Geology* **15**, 1143–1146.
- Mount, V. S., and J. Suppe (1992). Present-day stress orientations adjacent to active strike-slip faults: California and Sumatra, *J. Geophys. Res.* **97**, 11,995–12,013.
- Riddihough, R. P., and R. D. Hyndman (1991). Modern plate tectonic regime of the continental margin of western Canada, in *Geology of the Cordilleran Orogen in Canada*, H. Gabrielse and C. J. Yorath (Editors), Vol. 4, Geological Survey of Canada, Ottawa, Ontario, 435–455.
- Ristau, J., G. C. Rogers, and J. F. Cassidy (2007). Stress in western Canada from regional moment tensor analysis, *Can. J. Earth Sci.* **44**, 127–148.
- Rogers, G. C. (1983). Seismotectonics of British Columbia, *Ph.D. thesis*, University of British Columbia, 247 pp.
- Rogers, G. C. (1986). Seismic gaps along the Queen Charlotte fault, *Earthq. Predict. Res.* **4**, 1–11.

- Rohr, K. M. M. (2015). Plate boundary adjustments of the southernmost Queen Charlotte fault, *Bull. Seismol. Soc. Am.*, **105**, no. 2b, doi: [10.1785/0120140162](https://doi.org/10.1785/0120140162).
- Rohr, K. M. M., and L. Currie (1997). Queen Charlotte basin and Coast Mountains: Paired belts of subsidence and uplift caused by a low-angle normal fault, *Geology* **25**, 819–822.
- Rohr, K. M. M., and K. P. Furlong (1995). Ephemeral plate tectonics at the Queen Charlotte triple junction, *Geology* **23**, 1035–1038.
- Rohr, K. M. M., and A. J. Tryon (2010). Pacific-North America plate boundary reorganization in response to a change in relative plate motion: Offshore Canada, *Geochem. Geophys. Geosyst.* **11**, Q06007, doi: [10.1029/2009GC003019](https://doi.org/10.1029/2009GC003019).
- Rohr, K. M. M., C. Lowe, and P. D. Snively Jr. (1992). Seismic reflection, magnetics, and gravity data across the Queen Charlotte Fault and Dixon entrance, *Geol. Surv. Canada Open-File Rept.* 92-2615.
- Rohr, K. M. M., M. Scheidhauer, and A. M. Tréhu (2000). Transpression between two warm mafic plates: The Queen Charlotte Fault revisited, *J. Geophys. Res.* **105**, 8147–8172.
- Roland, E., N. Ruppert, S. Gulick, M. Walton, and P. Haeussler (2014). After-shocks following the January 5th 2013 Queen Charlotte–Fairweather Fault Earthquake near Craig, Alaska, *Seismol. Res. Lett.* **85**, no. 2, 466.
- Ruppert, N. A., H. Yue, and J. T. Freymueller (2014). Magnitude 7.5 earthquake of 5 January 2013 on Queen Charlotte Fault in Southeast Alaska, *Seismol. Res. Lett.* **85**, no. 2, 466.
- Sanderson, D. J., and W. R. D. Marchini (1984). Transpression, *J. Struct. Geol.* **5**, 449–458.
- Scheidhauer, M. (1997). Crustal structure of the Queen Charlotte transform fault zone from multi-channel seismic reflection and gravity data, *M.S. thesis*, Oregon State University, 184 pp.
- Scheidhauer, M., A. M. Tréhu, and K. M. M. Rohr (1999). Multichannel seismic reflection survey over the northern Queen Charlotte fault, *Geol. Surv. Canada Open-File Rept.* 99-3779.
- Schell, M. M., and L. J. Ruff (1989). Rupture of a seismic gap in southeastern Alaska: The 1972 Sitka earthquake (M_s 7.6), *Phys. Earth Planet. In.* **54**, 241–257.
- Shaw, J., and J. Suppe (1994). Active faulting and growth folding in the eastern Santa Barbara Channel, California, *Bull. Geol. Soc. Am.* **106**, 607–626.
- Smith, A. J., R. D. Hyndman, J. F. Cassidy, and K. Wang (2003). Structure, seismicity and thermal regime of the Queen Charlotte transform margin, *J. Geophys. Res.* **108**, 12, doi: [10.1029/2002JB002247](https://doi.org/10.1029/2002JB002247).
- Smith, W. H. F., and D. T. Sandwell (1995). Marine gravity field from declassified GEOSAT and ERS-1 altimetry, *Eos Trans. AGU* **76**, 46.
- Snively, P. D., Jr., H. C. Wagner, D. H. Tompkins, and D. L. Tiffin (1981). Preliminary geologic interpretation of a seismic reflection profile across the Queen Charlotte Island fault system off Dixon Entrance, Canada-United States, *U.S. Geol. Surv. Open-File Rept.* 81-299, 12 pp.
- Spence, G., and D. I. Long (1995). Transition from oceanic to continental crustal structure: Seismic and gravity models at the Queen Charlotte transform margin, *Can. J. Earth Sci.* **32**, 699–717.
- Stock, J. M., and P. Molnar (1988). Uncertainties and implications of the Late Cretaceous and Tertiary position of North America relative to the Farallon, Kula, and Pacific plates, *Tectonics* **7**, 1339–1384.
- Sylvester, A. G. (1988). Strike-slip faults, *Geol. Soc. Am. Bull.* **100**, 1666–1703.
- Tikoff, B., and C. Teyssier (1994). Strain modeling of displacement-field partitioning in transpressional orogens, *J. Struct. Geol.* **16**, 1575–1588.
- Titus, S. J., M. Dyson, C. DeMets, B. Tikoff, F. Rolandone, and R. Bürgmann (2011). Geologic versus geodetic deformation adjacent to the San Andreas fault, central California, *Geol. Soc. Am. Bull.* **123**, 794–820, doi: [10.1130/B30150.1](https://doi.org/10.1130/B30150.1).
- Titus, S. J., B. Housen, and B. Tikoff (2007). A kinematic model for the Rinconada fault system in central California based on structural analysis of en echelon folds and paleomagnetism, *J. Struct. Geol.* **29**, 961–982.
- Tschalenko, J. S. (1970). Similarities between shear zones of different magnitudes, *Geol. Soc. Am. Bull.* **81**, 1625–1640.
- Turcotte, D., and G. Schubert (1982). *Geodynamics: Applications of Continuum Physics to Geological Problems*, John Wiley and Sons, New York, New York, 450 pp.
- Vellutini, D., and R. M. Bustin (1991). Organic maturation of Mesozoic and Tertiary strata of the Queen Charlotte Islands, British Columbia, in *Evolution and Hydrocarbon Potential of the Queen Charlotte Basin, British Columbia*, G. Woodsworth (Editor), Paper 90-10, Geological Survey of Canada, Ottawa, Ontario, 411–451.
- Walcott, R. I. (1997). Modes of oblique compression: Late Cenozoic tectonics of the South Island of New Zealand, *Rev. Geophys.* **36**, 1–26.
- Wallace, R. E. (Editor) (1990). *The San Andreas fault system, CA, U.S. Geol. Surv. Prof. Pap.* 1515.
- Walton, M. A. L., S. P. S. Gulick, P. J. Haeussler, E. C. Roland, and A. M. Tréhu (2015). Basement and regional structure along-strike of the Queen Charlotte Fault in the context of modern and historical earthquake ruptures, *Bull. Seismol. Soc. Am.* **105**, doi: [10.1785/0120140174](https://doi.org/10.1785/0120140174).
- Walton, M. A. L., S. P. S. Gulick, R. S. Reece, G. A. Barth, G. L. Christeson, and H. Van Avendonk (2014). Dynamic response to tectonic control on the deposition and evolution of the Baranof Fan, Gulf of Alaska, *Geosphere* **10**, 13.
- Wessel, P., and W. H. F. Smith (1995). New version of the Generic Mapping Tools released, *Eos Trans. AGU* **76**, 329.
- Wilson, D. S. (2002). The Juan de Fuca plate and slab: Isochron structure and Cenozoic plate motions, in *The Cascadia Subduction Zone and Related Subduction Systems-Seismic Structure, Intralab Earthquakes and Processes, and Earthquake Hazards*, S. Kirby, K. Wang, and S. Dunlop (Editors), *U.S. Geol. Surv. Open-File Rept.* 02-328, 9–12.
- Yue, H., T. Lay, J. T. Freymueller, K. Ding, L. Rivera, N. A. Ruppert, and K. D. Koper (2013). Supershear rupture of the 5 January 2013 Craig, Alaska (M_w 7.5) earthquake, *J. Geophys. Res.* **118**, doi: [10.1002/2013JB010594](https://doi.org/10.1002/2013JB010594).

College of Earth, Ocean and Atmospheric Sciences (CEOAS)
Oregon State University
Admin. Building 104
Corvallis, Oregon 97331
trehu@coas.oregonstate.edu
(A.M.T., M.S.)

Kristin Rohr Consulting
719 Birch Road
N. Saanich BC V8L 5S1
Canada
(K.M.M.R.)

Department of Geoscience
University of Wisconsin-Madison
1215 W. Dayton Street
Madison, Wisconsin 53706
(B.T.)

The University of Texas Institute for Geophysics
J. J. Pickle Research Campus Building 196
10100 Burnet Road (R2200)
Austin, Texas 78758
(M.A.L.W., S.P.S.G.)

School of Oceanography
University of Washington
1503 NE Boat Street
Seattle, Washington 98105
(E.C.R.)